

THERMONUCLEAR BURSTS WITH SHORT RECURRENCE TIMES FROM NEUTRON STARS EXPLAINED BY OPACITY-DRIVEN CONVECTION

L. KEEK^{1,2} & A. HEGER^{3,4,5}

Abstract

Thermonuclear flashes of hydrogen and helium accreted onto neutron stars produce the frequently observed Type I X-ray bursts. It is the current paradigm that almost all material burns in a burst, after which it takes hours to accumulate fresh fuel for the next burst. In rare cases, however, bursts are observed with recurrence times as short as minutes. We present the first one-dimensional multi-zone simulations that reproduce this phenomenon. Bursts that ignite in a relatively hot neutron star envelope leave a substantial fraction of the fuel unburned at shallow depths. In the wake of the burst, convective mixing events driven by opacity bring this fuel down to the ignition depth on the observed timescale of minutes. There, unburned hydrogen mixes with the metal-rich ashes, igniting to produce a subsequent burst. We find burst pairs and triplets, similar to the observed instances. Our simulations reproduce the observed fraction of bursts with short waiting times of $\sim 30\%$, and demonstrate that short recurrence time bursts are typically less bright and of shorter duration.

Subject headings: accretion, accretion disks — methods: numerical — nuclear reactions, nucleosynthesis, abundances — stars: neutron — X-rays: binaries — X-rays: bursts

1. INTRODUCTION

Type I X-ray bursts are frequently observed from neutron stars that accrete through Roche-lobe overflow from a lower-mass companion star (for reviews, see Lewin et al. 1993; Strohmayer & Bildsten 2006; Galloway et al. 2008). The material accumulated on the neutron star surface is rich in helium and also hydrogen in most cases. Runaway thermonuclear burning in this layer produces an X-ray flash that typically lasts 10 – 100 s. It is the current paradigm that most of the accreted fuel is burned during a burst, with only a sliver of fuel remaining on top (e.g., Woosley et al. 2004; Fisker et al. 2008; José et al. 2010). The atmosphere must, therefore, be almost completely replaced by accretion before a new burst can ignite (see Woosley et al. 2004 for the effect of compositional inertia). Depending on the mass accretion rate, \dot{M} , X-ray bursts are observed to recur on timescales of hours, days, or even longer. An exceptional source is IGR J17480–2446, which has exhibited regularly repeating bursts with recurrence times as short as $t_{\text{recur}} \simeq 3.3$ min (Motta et al. 2011; Linares et al. 2012). There are, however, instances where the regularity is broken, and the distribution of t_{recur} is bimodal. At a constant \dot{M} , recurrence times of both a few hours and a few minutes appear.

Using the nomenclature of previous publications, we distinguish short waiting time (SWT) and long waiting time (LWT) bursts, depending on whether the time

since the previous burst was shorter or longer than 45 minutes, respectively (Boirin et al. 2007; Keek et al. 2010). LWT bursts have been observed to be followed by one (Murakami et al. 1980; Gottwald et al. 1987), two (Boirin et al. 2007), and even three SWT bursts (Galloway et al. 2008; Keek et al. 2010). Such events are referred to as double, triple, and quadruple bursts. Even when a source is in a state where it displays SWT bursts, many LWT bursts are not followed by an SWT burst (“single bursts”). The occurrence of SWT bursts appears to be random, with a $\sim 30\%$ probability for each burst (both LWT and SWT) to be followed by an SWT burst (Boirin et al. 2007; Keek et al. 2010). This suggests that a stochastic process is important for the ignition of SWT bursts.

Short recurrence times have been observed in rare cases from 15 sources (Keek et al. 2010). All sources are hydrogen-accretors with relatively high spin frequencies of $\nu \geq 549$ Hz. For individual sources it was found that SWT bursts are restricted to a range of \dot{M} , although the range does not always overlap for all sources, which may be due to the uncertainties in determining \dot{M} for each source. SWT bursts are typically less bright and less energetic than LWT bursts. Also, their shorter duration and the shape of their light curve indicate that SWT bursts are powered by fuel with a reduced hydrogen content compared to LWT bursts (Boirin et al. 2007).

With the mentioned exception of IGR J17480–2446, recurrence times of minutes are too short to accrete the fuel of an SWT burst. These bursts must be powered by fuel left-over from the previous burst. It has long been unexplained, however, how and where this fuel is preserved. The blackbody radius measured for the SWT and LWT bursts are consistent with being the same (Boirin et al. 2007), which disfavors explanations of this phenomenon that call on the burning of separate patches on the neutron star surface. Alternatively, fuel may be separated in layers at different depths in the atmosphere (Fujimoto et al. 1987). A second part of this puzzle is

laurens.keek@nasa.gov

¹ X-ray Astrophysics Laboratory, Astrophysics Science Division, NASA/GSFC, Greenbelt, MD 20771² CRESST and the Department of Astronomy, University of Maryland, College Park, MD 20742³ Monash Center for Astrophysics, School of Physics and Astronomy, Monash University, Victoria, 3800, Australia⁴ Shanghai Jiao-Tong University, Center for Nuclear Astrophysics, Department of Physics and Astronomy, Shanghai 200240, P.R. China⁵ University of Minnesota, School of Physics and Astronomy, Minneapolis, MN 55455

the reignition of this fuel on a short timescale. The short recurrence times vary between 3 min and 45 min (Keek et al. 2010): there is a considerable spread, even for SWT bursts from a single source, so it is unlikely to be related to a nuclear waiting point in the αp - and rp -processes, which would have a sharply defined time scale (Boirin et al. 2007).

In this paper we present one-dimensional models of the neutron star envelope, where SWT bursts are produced in a self-consistent manner with properties that closely reproduce many of the observed features. After introducing our numerical implementation (Section 2), we show models where a substantial fraction of the fuel survives the LWT burst, and is transported by convection to the ignition depth, producing an SWT burst on the observed timescale (Section 3). We compare the models to the observed SWT events, and discuss the accuracy of our convection implementation (Section 4), before presenting our conclusions (Section 5).

2. NEUTRON STAR ENVELOPE MODEL

We employ the successful burst model implemented in the hydrodynamics stellar evolution code KEPLER (Weaver et al. 1978; Woosley et al. 2004; Keek & Heger 2011; Keek et al. 2014). Here we describe the main properties of the model, and we refer to the cited papers for further details. An adaptive one-dimensional Lagrangian grid describes the outer layers of the neutron star in the radial direction. The base is formed by a 10^{25} g iron layer, on top of which material is accreted of solar composition (mass fractions of 0.71 ^1H , 0.27 ^4He , and 0.02 ^{14}N), since all observed SWT bursts are from hydrogen-rich sources (Keek et al. 2010). The outer zone has a mass of 10^{16} g. Accretion is implemented by using a finely resolved grid in the outer layers that is fixed relative to the surface. Advection of composition as well as compressional heating due to accretion is taken into account. Below a specified mass, which is chosen such that most nuclear reactions occur at greater depth, a fully Lagrangian grid is used (Keek & Heger 2011). In the present models, the specified mass corresponds to a column depth of $8 \times 10^6 \text{ g cm}^{-2}$.

We report the accretion rate of our simulations as a fraction of the Eddington-limited rate for solar composition: $\dot{M}_{\text{Edd}} = 1.75 \times 10^{-8} M_{\odot} \text{ yr}^{-1}$. Nuclear reactions are followed using a large adaptive network (Rauscher & Thielemann 2000; Rauscher et al. 2002) that includes the (“hot”) β -limited CNO cycle, the 3α , αp -, and rp -processes (Wallace & Woosley 1981). Neutrino losses from weak decays are taken into account. Chemical mixing due to convection uses mixing-length theory with a mixing-length parameter of $\alpha = 1$ and is implemented as a diffusive process (e.g., Clayton 1968). Semiconvection is modeled as a diffusive process with a diffusion coefficient that is 10% of that of thermal diffusion, similar in efficiency to the formulation by Langer et al. (1983) with an α value of 0.04. Thermohaline mixing is modeled following Heger et al. (2005), but mostly plays a minor role in the ashes layers.

Radiative opacity is implemented using analytic fits by Iben (1975) to numerical opacity calculations by Cox & Stewart (1970a,b), including electron scattering, Compton scattering, bound-free, and free-free transitions (see also Weaver et al. 1978). Furthermore, the opacity

due to electron conduction follows Itoh et al. (2008).

Pycno-nuclear as well as electron-capture reactions in the crust produce a heat flux into the neutron star envelope (Haensel & Zdunik 1990, 2003; Gupta et al. 2007). An unknown shallow heat source may add to this (Brown & Cumming 2009; Deibel et al. 2015; Turlione et al. 2015), whereas neutrino cooling by Urca cycling could reduce it (Schatz et al. 2014; Deibel et al. 2016). We calculate models for a range of values of the heating per accreted nucleon, Q_{b} , in units of MeV u^{-1} , with u the atomic mass unit, and set the luminosity at the inner boundary to $L_{\text{b}} = \dot{M} Q_{\text{b}}$.

The local gravity in our model is the Newtonian value for a $1.4 M_{\odot}$ neutron star with a radius of $R = 10$ km. The results presented in this paper are in the reference frame of the model domain. They can be corrected for General Relativistic effects (Keek & Heger 2011): keeping the gravitational mass of $1.4 M_{\odot}$, the same surface gravity is obtained including GR by increasing the stellar radius to $R = 11.2$ km, which produces a gravitational redshift of $z = 0.26$ (e.g., Woosley et al. 2004). For example, an observer at infinity will measure a t_{recur} that is 26% longer.

3. RESULTS

3.1. Simulations for a Range of Base Heating

We create 11 simulations with $\dot{M} = 0.1 \dot{M}_{\text{Edd}}$ for values of Q_{b} ranging from 0.1 MeV u^{-1} to 3.5 MeV u^{-1} . The simulations produce a series of on average 22 LWT bursts, and at the highest three values of Q_{b} both SWT and LWT bursts appear. The recurrence times of the two groups are sufficiently different to clearly distinguish the SWT from the LWT bursts (Figure 1). The shortest waiting time before an SWT burst is 4.6 min. The fraction of bursts that are SWT, f_{SWT} , increases with Q_{b} .

We determine the properties of the bursts in each simulation, excluding the first and the last burst. The recurrence time is measured as the time between the peaks in the luminosity of subsequent bursts; the fluence is measured by integrating the luminosity starting when it first exceeds 25% of the peak value up to the time it drops below $10^{36} \text{ erg s}^{-1}$. The size of the fuel column is determined by the location where the hydrogen mass fraction is reduced to 0.1 (compared to the accreted value of 0.71), and we give the value at the start and the end of the burst (“ignition” and “remainder” in Figure 1).

For all simulations, only part of the fuel column is burned by LWT bursts (Figure 1). For the coldest model, with $Q_{\text{b}} = 0.1 \text{ MeV u}^{-1}$, a fraction of $f_{\text{burn}} = 0.73$ of the fuel is burned, whereas for the largest Q_{b} a mere 25% is burned. The ignition column depth of the LWT bursts is smaller for larger Q_{b} and ranges from $1.16 \times 10^8 \text{ g cm}^{-2}$ to $0.67 \times 10^8 \text{ g cm}^{-2}$. The unburned remaining column exhibits a much smaller variation: for larger Q_{b} it increases from $0.51 \times 10^8 \text{ g cm}^{-2}$ to $0.56 \times 10^8 \text{ g cm}^{-2}$: whereas the relative fraction of unburned fuel increases with Q_{b} , the absolute amount of remaining fuel is similar in all cases. An important consequence is that the remaining fuel is closer to the ignition depth for larger Q_{b} .

If the entire fuel column needs to be replaced by accretion, the recurrence time is simply $t_{\text{recur}} = y_{\text{ign}}/\dot{m}$, with the specific mass accretion rate $\dot{m} = \dot{M}/4\pi R^2$ (in

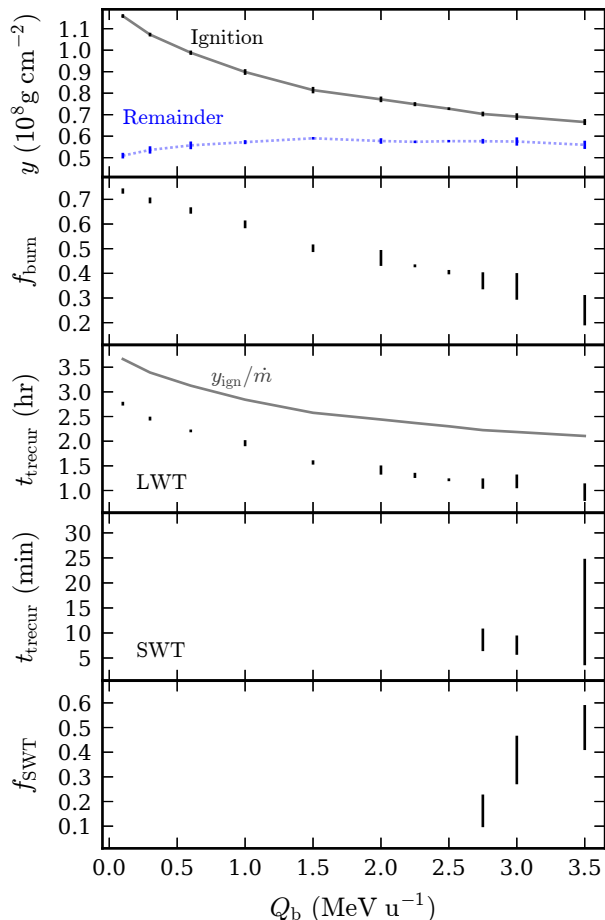


FIG. 1.— Properties of the bursts for a series of simulations with $\dot{M} = 0.1 \dot{M}_{\text{Edd}}$ as a function of the choice of base heating, Q_b . Shown are the column depths, y , where the LWT bursts ignite and where burning stops, leaving a remainder of unburned fuel; the fraction of the fuel burned in the LWT bursts, f_{burn} ; the recurrence times, t_{recur} , of the LWT and the SWT bursts, where for the former a solid line indicates the predicted values if all fuel had burned; the fraction of bursts that have a short waiting time, f_{SWT} , which is zero for all but the three largest values of Q_b . The error bars indicate the root mean squared variation of the quantities for a series of bursts in one simulation.

the Newtonian frame). We find, however, substantially shorter recurrence times even for the LWT bursts, as only the burned part of the column needs to be replaced by accretion (Figure 1).

3.2. Comparison of LWT and SWT Bursts

For $Q_b = 3.0 \text{ MeV u}^{-1}$, $f_{\text{SWT}} = 0.37 \pm 0.10$, which is consistent with the value of ~ 0.3 derived from observations (Boirin et al. 2007; Keek et al. 2010). The light curve of this simulation (Figure 2) looks qualitatively similar to the long exposures of the *XMM-Newton* and *Chandra* observatories on EXO 0748-676 (Boirin et al. 2007; Keek et al. 2010), with the appearance of burst doublet and triplet events seemingly at random. We employ this simulation to study the properties of the 24 LWT and 14 SWT bursts in more detail.

The bursts are divided among three categories: “single” bursts (LWT not followed by an SWT burst), “first” bursts (LWT followed by SWT), and SWT bursts. For

each burst we determine the fluence, peak luminosity, L_{peak} , and the ratio of the two, which gives the decay timescale, τ . The SWT bursts typically have a lower L_{peak} (Figure 3) and fluence (Figure 4) as well as a shorter τ (Figure 5). The distributions of these properties largely overlap for the single and first bursts. Interestingly, however, the highest values originate with single bursts. It indicates that when more fuel is consumed in an LWT burst, the subsequent appearance of an SWT burst is less likely.

The α -parameter is the ratio of the persistent fluence since the previous burst (including the accretion fluence) to the burst fluence. For the LWT bursts, we find values in the range of 47 to 66, with no notable difference in the distributions for single and first bursts. The SWT bursts have on average much lower α values ranging from 13 to 42.

When summing the fluence of each LWT burst and any following SWT bursts, we see that the combined fluence in double and triple events is as large as the most energetic single bursts (Figure 6), which is also an indication of the burning of left-over fuel in SWT bursts.

As mentioned, the properties of the LWT and SWT bursts in our simulation are qualitatively similar to those observed from EXO 0748-676 (see Figure 7 of Boirin et al. 2007) as well as a large compilation of observations of bursting sources (compare with Figures 9-12 of Keek et al. 2010). For the latter, the combination of multiple sources and a wide range of mass accretion rates produces histograms with broader distributions than our simulation at a constant mass accretion rate. Nonetheless, we see the same behavior, with SWT bursts being on average less bright and of shorter duration than LWT bursts, and the summed fluence in multiple-burst events being comparable to the fluence of the more energetic single bursts.

3.3. Detailed Look at a Burst Triplet

To investigate the processes that produce SWT bursts, we study one triplet burst in detail, which we take from the simulation with $Q_b = 3.0 \text{ MeV u}^{-1}$ (see at 6.7 hr in Figure 2). Its light curve exhibits 3 bursts as well as a series of smaller bumps (Figure 7). The bumps originate from mixing events near the burst ignition depth, and involve a small amount of localized burning. In contrast, nuclear burning is stronger during the bursts, spreading from the ignition location to smaller depth, and powering a flare that is over an order of magnitude brighter than a bump. With a peak luminosity of $\lesssim 10\%$ of the accretion luminosity, it will be challenging to detect these bumps in X-ray observations (Figure 2).

Comparing the light curves of the three bursts, we see that the first burst is the brightest with a long tail that shows a substantial contribution from the *rp*-process, as evidenced by the “hump” around ~ 50 s (Figure 8). The subsequent SWT bursts have a lower L_{peak} , a smaller fluence, and a shorter duration, which we found to be typical for SWT bursts in our simulations (Section 3.2).

3.3.1. Incomplete burning

The waiting time before the LWT burst was 1.03 hr, during which a column of $\Delta y = 0.32 \times 10^8 \text{ g cm}^{-2}$ was accreted. Burst ignition occurs deeper at $y_{\text{ign}} = 0.65 \times$

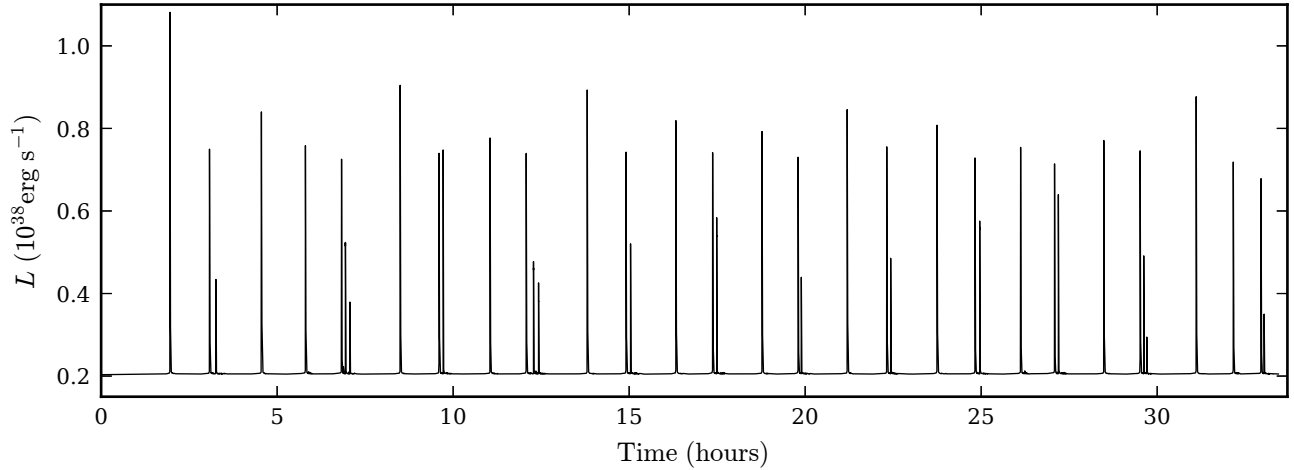


FIG. 2.— Both LWT and SWT bursts are visible in the light curve of a simulation with $\dot{M} = 0.1\dot{M}_{\text{Edd}}$ and $Q_b = 3.0 \text{ MeV u}^{-1}$. The accretion luminosity of $0.2 \times 10^{38} \text{ erg s}^{-1}$ is included. The qualitative bursting behavior is strikingly similar to that seen during long observations of EXO 0748-676 (Boirin et al. 2007; Keek et al. 2010).

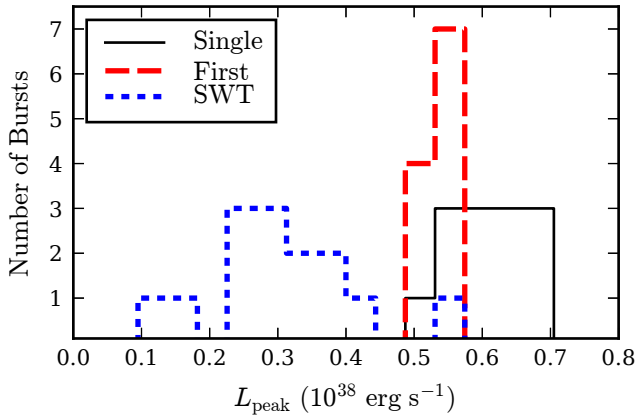


FIG. 3.— Histogram of the peak luminosity, L_{peak} , for single bursts, the first bursts of multiple events, and SWT bursts from Figure 2. The SWT bursts are typically less bright than the LWT bursts.

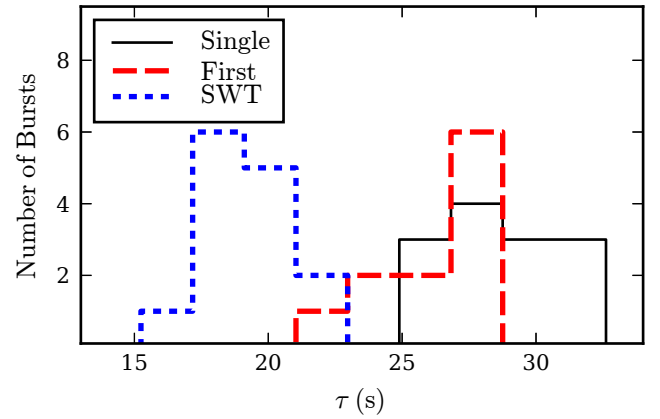


FIG. 5.— Histogram of the decay time scale, τ , (the ratio of the burst fluence to the peak luminosity) for the same burst categories as Figure 3. The SWT bursts last shorter than the LWT bursts.

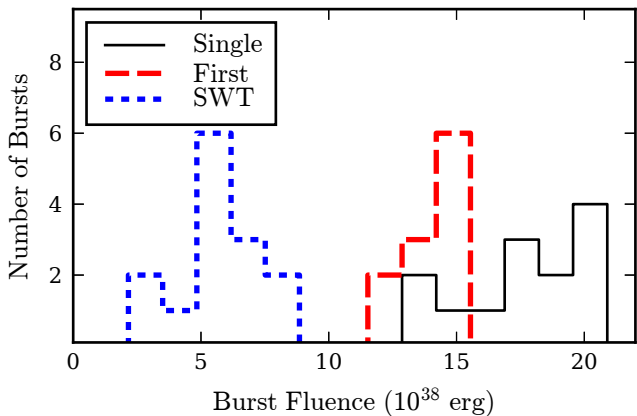


FIG. 4.— Histogram of the burst fluence for the same burst categories as Figure 3. The SWT bursts are less energetic than the LWT bursts.

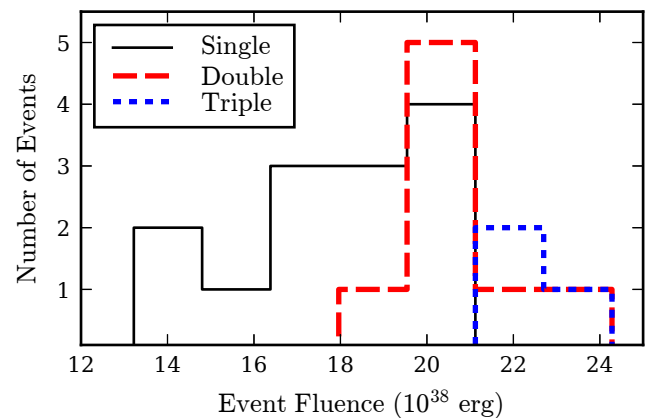


FIG. 6.— Histogram of the fluence of burst events, i.e., where we sum the fluence of two bursts in a double or three in a triple event. The distributions for double and triple are consistent with the highest values for single, which suggests that SWT bursts are powered by left-over fuel.

10^8 g cm^{-2} : material that was accreted prior to the preceding burst is pushed deeper by the fresh fuel on top, and this material now ignites a burst. We track the to-

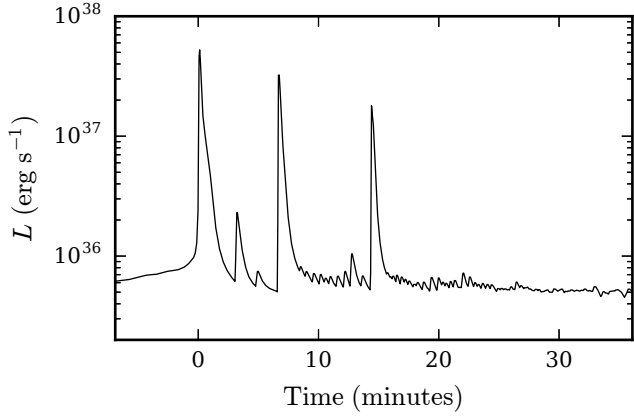


FIG. 7.— The light curve of the triple burst event at 6.7 hr in Figure 2 (the accretion flux is not included here). Aside from the three bursts, smaller bumps are visible due to convective mixing events.

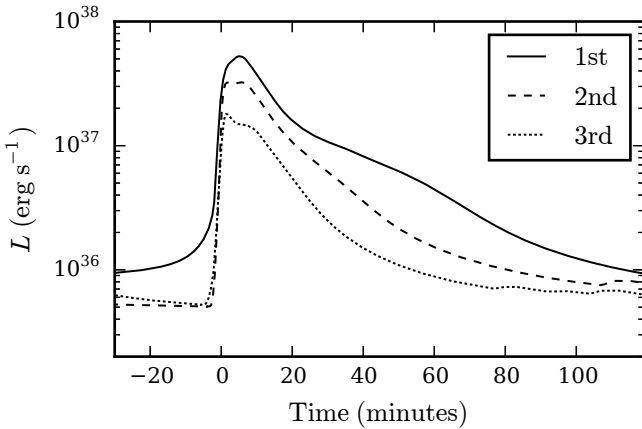


FIG. 8.— Comparison of burst profiles of the triple burst in Figure 7. The light curves have been shifted in time such that their rises coincide at 0.

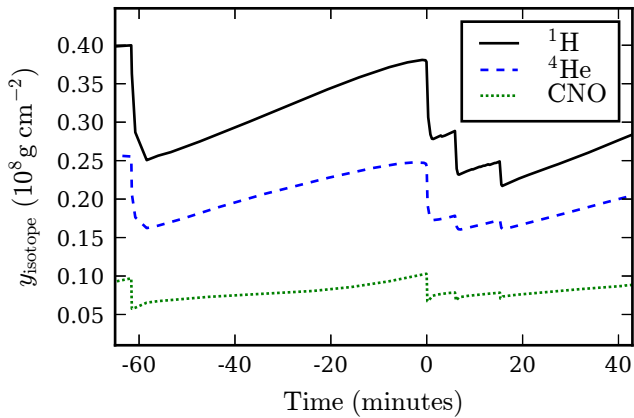


FIG. 9.— Total mass column of hydrogen, helium, and the combined CNO isotopes for the triple burst in Figure 7. After the previous burst on the left-hand side, accretion slowly increases the fuel column over time, whereas the three bursts cause sudden decreases. After each burst in the triplet, accretion does not fully compensate for the burned fuel burned before the next burst ignites.

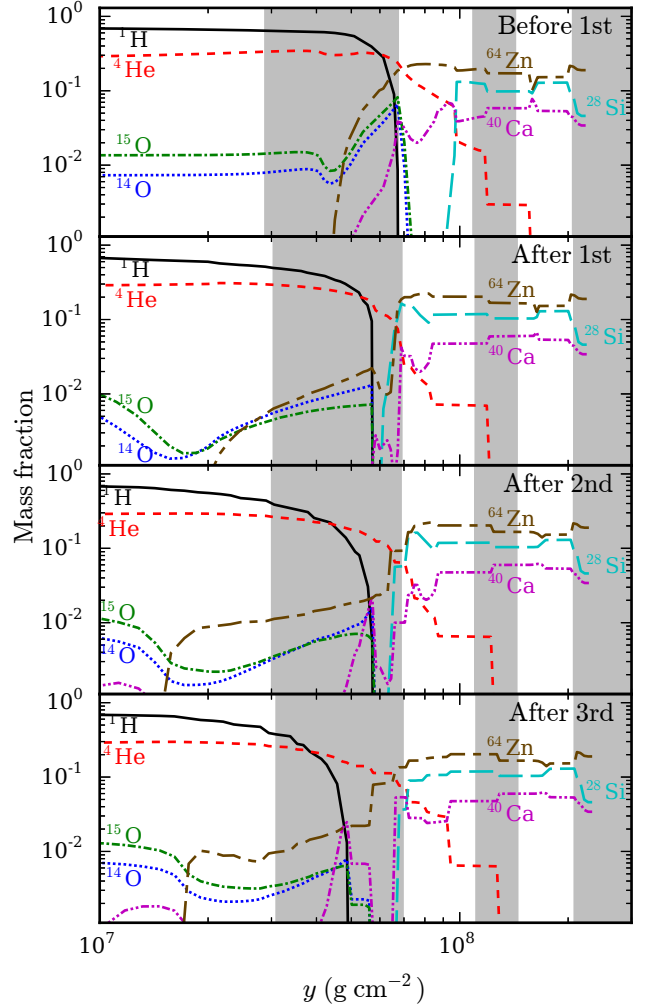


FIG. 10.— Composition of the envelope 1 min before the burst triplet and 2 min after each of the three bursts. Shown are the mass fractions as a function of column depth, y , for a small selection of the most abundant isotopes. Alternate white and gray shaded areas correspond to the layers accreted between subsequent LWT bursts, and the small offsets visible between the panels are due to small amounts of accretion between the shown instances. At large depths (on the right-hand side) is the outer part of the iron substrate of the model.

tal column of hydrogen, helium, and CNO in the model as a function of time (Figure 9). After the first burst, a substantial fraction of hydrogen and helium remains. Accretion slowly increases their columns over time, but this increase is minor in the short waiting time before the SWT bursts. Reignition involves, therefore, left-over fuel instead of fresh fuel. The amount of fuel burned is smaller for each successive burst. The amount of helium burned in the SWT bursts is relatively small. Furthermore, the small reduction in the CNO column during the SWT bursts, is quickly compensated by 3α burning after the bursts.

We take a closer look at the composition as a function of depth at several times: before the LWT burst and after each of the three bursts (Figure 10). Ignition of the LWT burst takes place close to the bottom of the hydrogen column, which is also close to the bottom of the layer that was accreted before the *previous* LWT burst. Furthermore, the ignition location contains ashes

of the previous burst. The most abundant heavy isotope is ^{64}Zn , which is produced by the *rp*-process, and some α elements such as ^{40}Ca are present with smaller mass fractions. These ashes produce so-called compositional inertia (Woosley et al. 2004), which reduces the recurrence time of bursts (e.g., in Figure 2 the waiting time before the first burst is longer than for the others). Near y_{ign} the hydrogen mass fraction has been reduced by βCNO burning before the LWT burst. After each subsequent burst, the hydrogen column is further reduced. Moreover, the steepness of the hydrogen profile is reduced, mostly by the mixing events in between the bursts. The SWT bursts, therefore, are primarily powered by hydrogen that is already available at the start of the LWT burst.

Before the LWT burst, the CNO abundance peaks at the bottom of the hydrogen column (Figure 10). After this burst, the CNO mass fractions are reduced at smaller column depths. The lack of CNO inhibits hydrogen burning at smaller column depth, facilitating its survival.

Each burst sends a heat wave into the deeper layers, inducing α -captures that produce isotopes such as ^{28}Si (see also Woosley et al. 2004).

3.3.2. Reignition

Figure 11 presents a detailed view of the location of hydrogen fuel during the burst triplet. After each burst a series of brief convective mixing events occur. Convection takes place in the ashes layer directly below the left-over hydrogen. Convective overshooting extends the mixing region, dragging hydrogen down into the ashes layer. This causes a small amount of burning and shuts off convection. Subsequent mixing events bring hydrogen to larger column depths. For all three bursts, ignition occurs near the same depth $y_{\text{ign}} = 0.65 \times 10^8 \text{ g cm}^{-2}$ (Figure 11). Once the convective events reach this depth, the mixed-in fuel ignites as a new burst.

In order to understand why the mixing events occur, consider the evolution of several quantities at y_{ign} (Figure 12). During each burst, nuclear burning (indicated by the specific nuclear energy ϵ_{nuc}) depletes hydrogen at this depth, and strongly raises the temperature, T . This is followed by several minutes of cooling, which lowers T back down. The temperature and composition changes have a strong effect on the opacity, κ . Comparing κ before and after the first burst shows the effect of burning all hydrogen. The compositional changes are less radical for the SWT bursts, but the temperature evolution induces changes in κ of similar magnitude. To illustrate the temperature dependence, we calculate κ for a range of temperatures, using the properties of the model at y_{ign} and $t = 5$ minutes after the LWT burst (Figure 13). Within the range of temperatures spanned in our triple burst, cooling clearly produces an increase in the opacity. In fact, κ peaks in the ashes layer around y_{ign} (Figure 14), and there is a steep drop in κ between the ashes layer and the hydrogen-rich layer. An increase in κ makes radiative cooling less efficient, and convection sets in when $\kappa \gtrsim 0.4 \text{ cm}^2 \text{ g}^{-1}$.

As κ peaks in the ashes layer right below the hydrogen-rich layer, convective mixing takes place close to the left-over fuel. Turbulent mixing can “overshoot” into neighboring zones, and this brings hydrogen into the ashes

layer. Some of the protons capture onto the metals in the ashes. This produces a small peak in ϵ_{nuc} and an equivalent increase in T , which reduces κ (Figure 12). As convection is switched off, this marks the end of one mixing event. After radiative cooling decreases T and increases κ once again, a next convective mixing event initiates. In this way, each burst is followed by a series of brief mixing events. Each event brings hydrogen to larger y , but only when y_{ign} is reached, does a full burst ignite.

After the first burst, only two mixing events were required to ignite the second burst, but ten occurred before the third burst. The last burst was followed by an even larger number of mixing events, but no fourth burst appeared. One reason for this is that each subsequent burst depletes hydrogen further from y_{ign} (Figure 10, 11), thus requiring mixing to bridge an increasing Δy . Another aspect is the steepness of the hydrogen profile, which is reduced by each burst (Figure 10). After later bursts, the hydrogen content of the mixed-in material is lower, and each mixing event transports hydrogen over a smaller Δy . The mixing events after the first burst provide each $\Delta y \simeq 2.9 \times 10^6 \text{ g cm}^{-2}$, whereas after the second burst $\Delta y \simeq 1.1 \times 10^6 \text{ g cm}^{-2}$, and after the third burst $\Delta y \simeq 0.8 \times 10^6 \text{ g cm}^{-2}$ (Figure 11). The later mixing events bring in a smaller amount of hydrogen, powering weaker burning events, which provide smaller temperature increases, halting convection for a shorter time. The time between subsequent mixing events is 2.9 minutes after burst one, ~ 0.8 minutes after two, and ~ 0.4 minutes after three, respectively.

As mentioned, during the convective episodes, a small fraction of the mixed-in hydrogen burns by proton capture on available seed nuclei in the ashes of the previous burst. When y_{ign} is reached, however, there is a notable difference in the nuclear burning processes. The nuclear flow through the βCNO cycle breakout reactions $^{15}\text{O}(\alpha, \gamma)^{19}\text{Ne}$ and $^{18}\text{Ne}(\alpha, p)^{21}\text{Na}$ exceeds the 3α flow (Figure 12). CNO is removed faster than it is created, while producing new seed nuclei for the *ap*- and *rp*-processes. This leads to runaway burning that spreads to neighboring zones, resulting in an SWT burst.

3.4. Alternative Simulations: Enhanced Convection

We perform similar simulations at $\dot{M} = 0.05 \dot{M}_{\text{Edd}}$, $\dot{M} = 0.2 \dot{M}_{\text{Edd}}$, and $\dot{M} = 0.3 \dot{M}_{\text{Edd}}$, but do not find SWT bursts. This suggests that SWT bursts are confined to a narrow range of \dot{M} around $\dot{M} = 0.1 \dot{M}_{\text{Edd}}$.

As an alternative to the strong base heating, we investigate the effect of enhancing the strength of convective mixing. We assume $Q_{\text{b}} = 0.1 \text{ MeV u}^{-1}$ and scale the mixing length diffusivity by a factor f_{diff} . This is equivalent to increasing the length scale over which convective mixing takes place. For $\dot{M} = 0.1 \dot{M}_{\text{Edd}}$ no SWT bursts are found for $1 \leq f_{\text{diff}} \leq 100$ at accretion rates of $\dot{M} = 0.1 \dot{M}_{\text{Edd}}$, $\dot{M} = 0.2 \dot{M}_{\text{Edd}}$, and $\dot{M} = 0.3 \dot{M}_{\text{Edd}}$. At $\dot{M} = 0.05 \dot{M}_{\text{Edd}}$, we find SWT bursts for $f_{\text{diff}} > 5$, with SWT fractions ranging from 0.1 to 0.4 (Figure 15). Even without strong heating, also for $Q_{\text{b}} = 0.1 \text{ MeV u}^{-1}$ a substantial amount of fuel is left unburned after an LWT burst (Figure 1). The distance between the left-over fuel and the ignition location is larger for smaller Q_{b} , but in this case the stronger convection has a suffi-

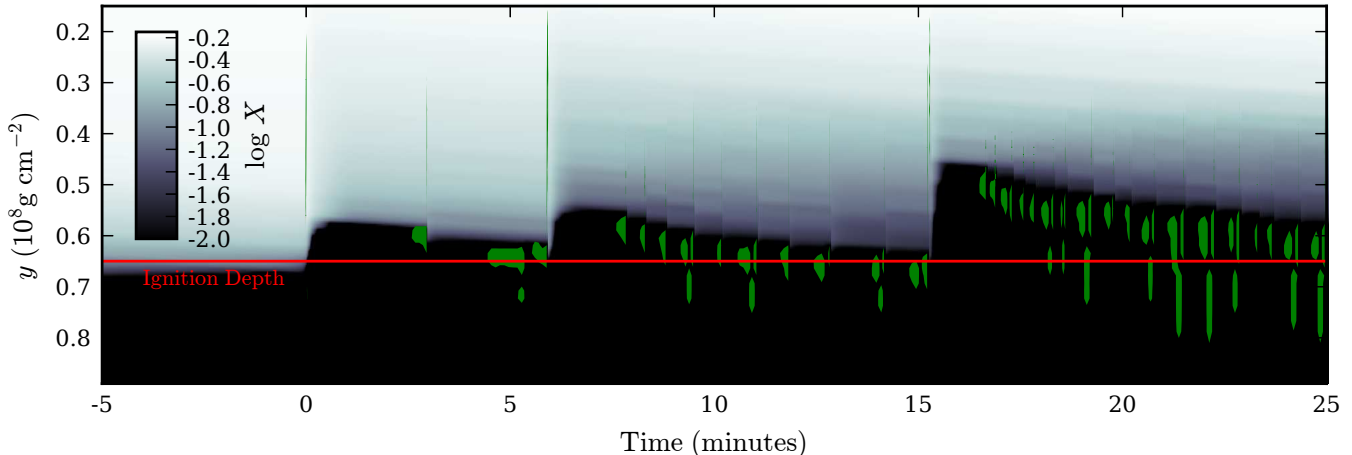


FIG. 11.— The hydrogen mass fraction, X , as a function of time and column depth, y , during the burst triplet from Figure 7. Accreted material is on top, and burst ashes are at the bottom. The horizontal line indicates the ignition depth (y_{ign}) of the three bursts, and the green areas mark convective regions. Mixing transports hydrogen in steps down to y_{ign} , where it ignites and powers the SWT bursts.

ciently long reach.

4. DISCUSSION

SWT bursts have first been observed shortly after the discovery of Type I bursts (Lewin et al. 1976). Based on the relatively small sample of bursts observed with *EXOSAT*, Fujimoto et al. (1987) thought of SWT and LWT bursts as part of a continuous distribution of recurrence times, and sought to understand them using a single ignition mechanism. A much larger burst sample observed with the *Rossi X-ray Timing Explorer* (Galloway et al. 2008) and the *BeppoSAX* Wide Field Cameras (Cornelisse et al. 2003) was compiled in the Multi-Instrument Burst Archive (MINBAR), and it revealed a distinctly bimodal distribution of t_{recur} (Keek et al. 2010). Furthermore, day-long observations with *XMM-Newton* and *Chandra* (Boirin et al. 2007; Keek et al. 2010) showed that the bimodality is intrinsic to the source, rather than an artifact from observing in low-Earth orbit, where Earth occultations typically allow for at most ~ 60 minutes of uninterrupted observation of a source. The bimodality indicates that LWT and SWT bursts reach ignition in a different way, which is confirmed by our simulations. In this section we discuss the issues of left-over fuel and its reignition, comparing previous suggested scenarios to our fully self-consistent numerical models.

4.1. Left-Over Fuel

Fujimoto et al. (1987) considered the fast transport of freshly accreted fuel down to y_{ign} , but realized that for SWT with $t_{\text{recur}} < 10$ minutes there is insufficient time to accrete sufficient material. Unburned fuel must remain after a burst to power an SWT burst.

Boirin et al. (2007) noted the difficulty in explaining the recurrence time of the LWT bursts from EXO 0748-676, as it appeared short compared to the expected accretion time scale. They considered both hydrogen-ignited and helium-ignited burst scenarios, and found that both explanations required the source distance to be at either extreme of the observationally allowed range. Assuming a larger distance results in a higher accretion luminosity

and a shorter accretion time scale. This was, however, based on ignition models that assume the whole ignition column needs to be replaced before the next burst. If only a fraction f_{burn} is consumed, the expected recurrence time is reduced by a factor f_{burn} as well. The fact that some fuel is left-over, therefore, also has an observable effect on the LWT bursts.

A third observational indication for the burning of left-over fuel is the low α -parameter measured for SWT bursts. This parameter is the ratio of the persistent fluence between subsequent bursts to the burst fluence, and it provides a measure of how much is accreted versus burned. The SWT bursts have anomalously low values of $\alpha \lesssim 20$ (Boirin et al. 2007). For example, assuming the accretion of pure hydrogen which all burns to iron in a burst, the minimum expected value is $\alpha \simeq 20$. This again indicates that the burst fuel was not accreted within the short recurrence time. The α values for the LWT bursts have typical values (Boirin et al. 2007), which may be understood if both the persistent and burst fluence are reduced by the same factor f_{burn} . In our simulations we find α values as low as 13 for the SWT bursts, whereas $\alpha \geq 47$ for the LWT bursts (Section 3.2).

In our series of simulations, roughly the same column of fuel remains after each LWT burst (Figure 1). As these are relatively weak bursts (the luminosity does not reach the Eddington limit), the convection zone at the burst onset is short-lived, and the extent of the burning region is largely set by the local conditions at each depth (see also Woosley et al. 2004). Therefore, a similar absolute amount of fuel is left over in all models. The more important distinction is that for models with stronger base heating (a larger Q_b), y_{ign} is reduced, which increases the relative amount of unburned fuel. For the LWT bursts, t_{recur} is substantially lower than the expectation when all fuel burns (Figure 1). Moreover, when y_{ign} is closer to the left-over fuel, it is easier to transport this fuel to the location where it can ignite to produce an SWT burst. Indeed, our simulations exhibit SWT bursts for $Q_b \geq 2.75 \text{ MeV u}^{-1}$. Such large values cannot be provided by crustal heating (Haensel & Zdunik 2003; Gupta et al. 2007), but the dissipation of rota-

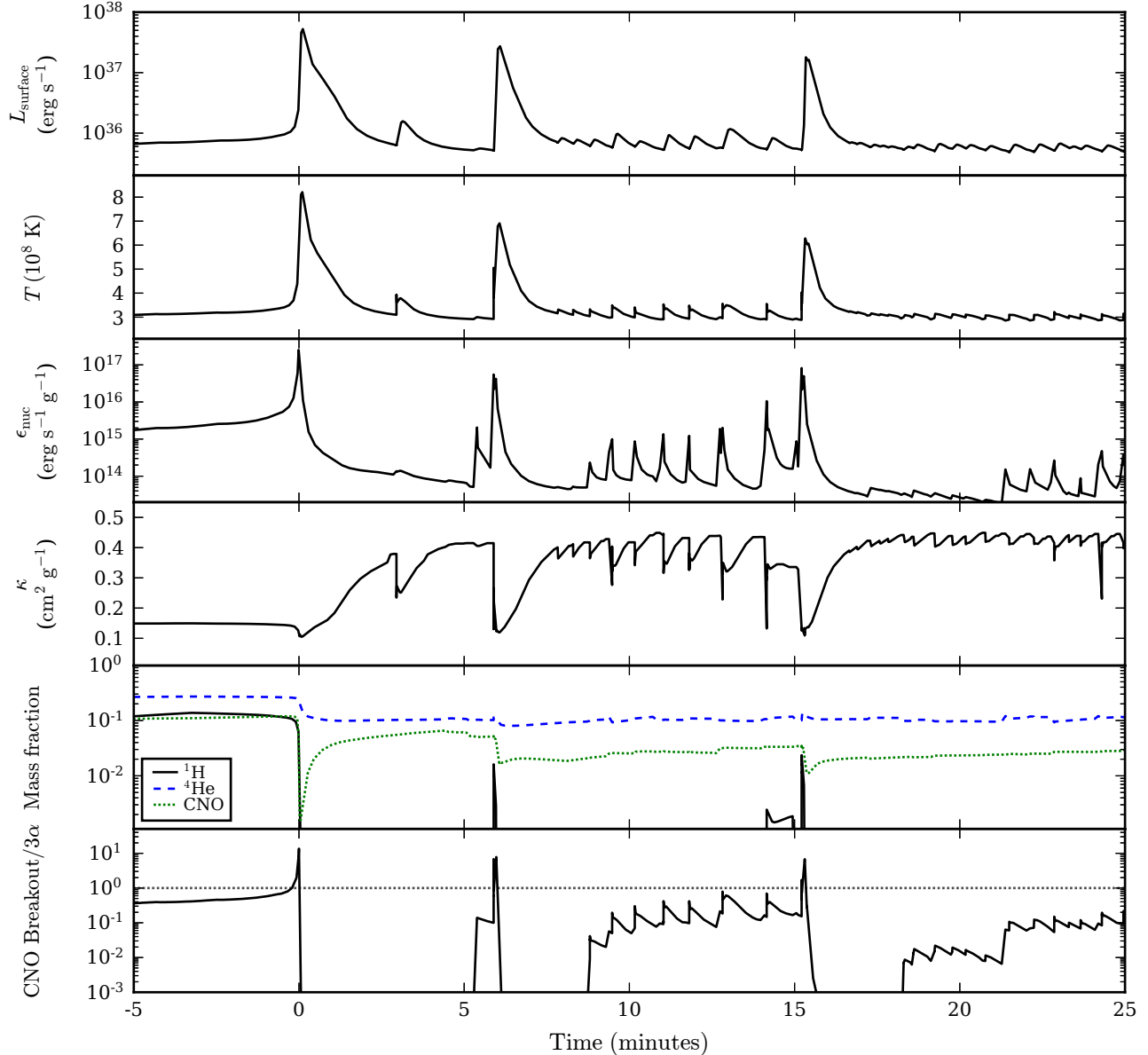


FIG. 12.— Properties of the triple burst event in Figure 7 as a function of time since the start of the first burst. The top panel shows the surface luminosity L_{surface} , whereas the other panels show properties at the ignition depth of $y_{\text{ign}} = 0.65 \times 10^8 \text{ g cm}^{-2}$: temperature T , specific nuclear energy generation rate ϵ_{nuc} , opacity κ , mass fractions of hydrogen helium and the combined CNO elements, and the ratio of the nuclear flows through the β CNO breakout reactions ($^{15}\text{O}(\alpha, \gamma)^{19}\text{Ne}$ and $^{18}\text{Ne}(\alpha, p)^{21}\text{Na}$) to the 3α reaction. In the bottom panel the dotted horizontal line indicates unity, showing that only during the three bursts does breakout flow exceed the 3α flow.

tional energy potentially is a source of substantial heating (Inogamov & Sunyaev 2010).

4.2. Turbulent Reignition

Boirin et al. (2007) noted that all sources that exhibit SWT bursts have a fast spinning neutron star, suggesting the importance of rotationally induced processes, such as rotational mixing. Rotationally induced mixing was also proffered by Fujimoto et al. (1987) as the mechanism to transport fuel to y_{ign} on a faster timescale than the accretion timescale. The timescale for this mixing process may indeed be similar to the SWT recurrence time (Fujimoto 1988). Since this mixing process is active continuously, however, it would produce SWT bursts all the

time (Piro & Bildsten 2007), or even stabilize the burning (Keek et al. 2009), whereas we observe both SWT and LWT bursts.

Our simulations do not include rotational mixing. Instead, left-over fuel is transported to y_{ign} by convection. Woosley et al. (2004) noted “interesting episodes of convection in between the bursts.” These convective mixing events occur in the ashes layer on a timescale of minutes following a burst. The turbulence may extend beyond the region where the Ledoux criterion is met, which is known as convective overshooting. This process can grab hydrogen-rich left-over fuel and bring it to greater depth. We find that several of such mixing events are required

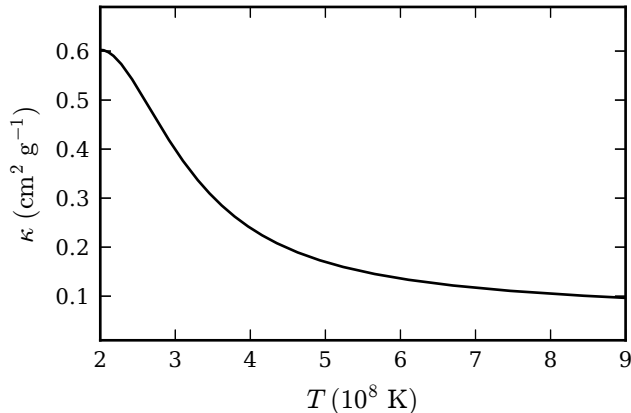


FIG. 13.— Opacity, κ , as a function of temperature, T . We take the model at $t = 5$ minutes and the zone at y_{ign} (Figure 12), which is devoid of hydrogen and has a density of $\rho = 5.3 \times 10^5 \text{ g cm}^{-3}$, and we calculate κ in the range of T that is relevant for the triple burst (Figure 12). The density dependence is small: for this zone $\rho = (2.7 - 5.4) \times 10^5 \text{ g cm}^{-3}$, which produces $\kappa = 0.37 - 0.41 \text{ cm}^2 \text{ g}^{-1}$.

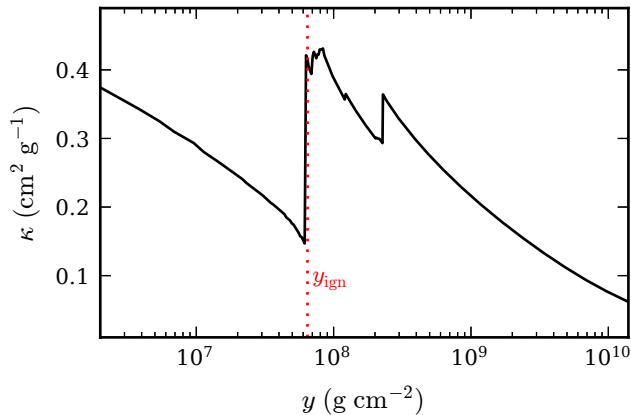


FIG. 14.— Opacity, κ , as a function of column depth, y , for the model at $t = 5$ minutes (Figure 12). The ignition depth, y_{ign} , is indicated by the dotted line. Close to this depth, there is a sharp jump in κ , from the H-rich region at smaller depth to the H-depleted ashes at larger depth. κ has a maximum around y_{ign} , and here convection sets in. Towards larger depths, κ exhibits small steps at the boundaries of the different ashes layers, and the largest step is at the iron substrate (see also Figure 10).

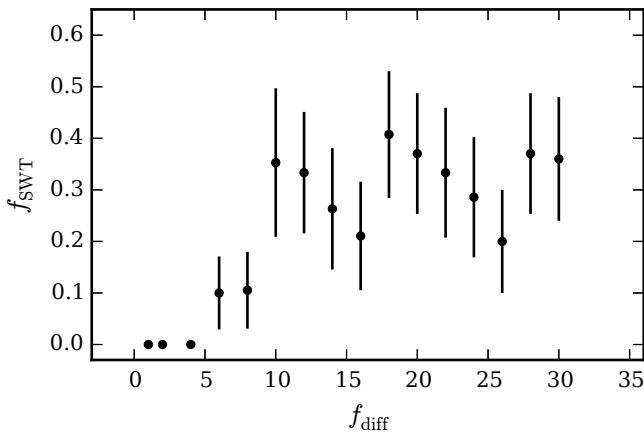


FIG. 15.— SWT fractions of models as a function of diffusivity scale factor f_{diff} for $\dot{M} = 0.05 \dot{M}_{\text{Edd}}$ and $Q_b = 0.1 \text{ MeV u}^{-1}$.

to transport the fuel to y_{ign} , where it ignites an SWT burst (Figure 11). The stochastic nature of convection provides a natural explanation for the fact that SWT bursts seemingly occur at random with a $\sim 30\%$ probability. Furthermore, the left-over fuel is mixed with the ashes, such that the burst results from burning a diluted composition. This is consistent with the lower hydrogen content inferred from observations (Boirin et al. 2007). Each SWT burst depletes hydrogen to smaller depths, and a sequence of mixing events progressively dilutes the fuel with ashes. Over time, it is increasingly difficult to bring sufficient hydrogen down to y_{ign} to ignite an SWT burst. Small mass fractions of hydrogen burn away without triggering a runaway. This limits the number of subsequent SWT bursts in our simulations to at most two. Afterwards, accretion slowly replaces the burned material, and an LWT burst ignites. The largest observed number of subsequent SWT bursts was three for a quadruple event from 4U 1636-536 (Keek et al. 2010). The first SWT burst was rather underluminous, which may explain why it could be followed by two more SWT bursts.

The convective mixing events are caused by an anti-correlation of the opacity and temperature. The free-free opacity depends on temperature as $\kappa_{\text{ff}} \propto T^{-7/2}$ (e.g., Kippenhahn & Weigert 1994). The total opacity in our model, which further includes contributions from, e.g., electron scattering, also exhibits this anti-correlation, albeit with a slightly less steep slope (Figure 13). During the cooling phase following a burst, the T decrease leads to an increase in κ . As radiative energy transport becomes less efficient, convection sets in. Convection not only transports heat outwards, but also mixes the composition inwards. The opacity peaks in the ashes layer close to the unburned fuel. Convective overshooting, therefore, drags hydrogen-rich material into the ashes layer. Some of the protons are quickly captured onto seed-nuclei in the ashes. These capture reactions increase T and consequently lower κ . Convection switches off as energy transport becomes radiative again. Another cooling phase follows, leading up to the next convective mixing event. The result is the periodic switching on and off of convection on a cooling timescale of a few minutes. This behavior is reminiscent of the κ -mechanism that produces pulsations in Cepheids, where the anti-correlation between T and κ drives expansion and contraction (e.g., Cox & Whitney 1958). The neutron star envelope acts as a thin shell, where the strong gravitational pull of the neutron star inhibits substantial expansion. Instead, the anti-correlation between T and κ drives the mixing events and the burning of hydrogen.

4.3. Model Accuracy and Improvements

Next, we discuss how our results depend on the implementation of our code, in particular with respect to the opacity and convective mixing. For the conditions relevant for the bursts in our models, the most important contributions to the opacity are from electron scattering and free-free transitions. They are implemented following the numerical opacity calculations by Cox & Stewart (1970a,b) (see also Section 2). Obtaining more accurate opacities is challenging, because of the wide range of compositions present in the models, from solar to many different mixtures of hydrogen, helium, and a wide range of

metals. The required mixtures are typically not covered by modern opacity tables (e.g., OPAL; Iglesias & Rogers 1996). Cox (1965) found the differences between opacity calculations as well as fits to calculations to be of the order 10% – 30%. We, therefore, expect the uncertainties in our opacity implementation to be at least of this size. A systematic shift in κ influences the conditions when convection switches on or off.

Convective mixing is implemented as a diffusive process using mixing length theory. We find that the SWT phenomenon strongly depends on the length scale over which mixing takes place, which is only approximated in our model. For example, our simulations with $Q_b = 0.1 \text{ MeV u}^{-1}$ present the largest distance between y_{ign} and the left-over fuel (Figure 1). When the convective length scale is increased by a factor 10, SWT bursts appear (Figure 15), although at a lower \dot{M} .

Of special importance is convective overshooting. In our model, overshooting crucially mixes hydrogen into the ashes layer. When turned off, no SWT bursts occur. The length scale over which mixing by convective overshooting takes place, l_{mix} , is often assumed to be proportional to the pressure scale height H_P , although the precise value is highly uncertain: $l_{\text{mix}} \simeq (0.1 - 10)H_P$ (e.g., Zhang 2013). Our implementation of overshooting is, however, crude: mixing is extended one zone beyond the boundaries of the convective region. In tests where we reduce the zone size, the amount of hydrogen mixed into the ashes is decreased, and the SWT bursts disappear. Multi-dimensional hydrodynamics models are required to improve our understanding of the length scales of convection and convective overshooting, for example with the recently developed MAESTRO code (Malone et al. 2011, 2014; Zingale et al. 2015). Methods may be developed to use multi-dimensional simulations to inform improved implementations of turbulent mixing in one-dimensional models (e.g., Arnett et al. 2015). For example, one-dimensional turbulence (ODT; Kerstein 1991) models employ a stochastic approach.

For individual sources, SWT burst observations are restricted to a range of mass accretion rates. This is also the case in our simulations. This may be understood because at lower \dot{M} , y_{ign} is larger, so f_{burn} is higher (see Figure 1), and most (all) hydrogen burns in the βCNO cycle. Therefore, it is harder to mix hydrogen down to y_{ign} . For the observed sources, the upper bound coincides with a change in the state of the accretion disk and an accompanying change in the burst regime (Galloway et al.

2008; Keek et al. 2010). Such a state transition is, however, not part of our model. The lack of SWT bursts at $\dot{M} \geq 0.2 \dot{M}_{\text{Edd}}$ needs to be investigated further, but we may find it to be due to the approximate prescription of convective mixing and overshooting in our model.

In summary, our models convincingly reproduce the qualitative behavior of SWT bursts in great detail. Improvements in the implementation of convection and convective overshooting are, however, crucial in accurately predicting the quantitative properties of SWT bursts, including the range of \dot{M} and Q_b where they occur.

5. CONCLUSIONS

We present the first one-dimensional numerical models that include X-ray bursts with both regular long recurrence times and recurrence times as short as ~ 5 minutes. The observed behavior of these bursts is qualitatively reproduced in great detail: bursts appear in single, double, or triple events; the SWT bursts are shorter, less bright, and less energetic than the LWT bursts; SWT bursts occur at $\dot{M}/\dot{M}_{\text{Edd}} = 0.05 - 0.1$; the observed fraction of SWT bursts of $\sim 30\%$ is reproduced. We find that SWT bursts occur when after a burst some hydrogen-rich fuel is left unburned at smaller column depth, and a series of convective mixing events brings it down to the ignition depth, where a new burst ignites. Strong base heating lowers the burst ignition depth, reducing its distance from the left-over fuel, which makes it easier to produce an SWT burst. The opacity in the ashes layer is anti-correlated with the temperature, such that after a cooling timescale of a few minutes, the ashes become opaque, and a convective mixing event initiates. The implementation of convection and convective overshooting in one-dimensional codes is rather crude. Improvements in this area are crucial to accurately predict the mass accretion rates and amount of base heating that is required to produce SWT bursts.

The authors are grateful to Jean in 't Zand, Tod Strohmayer, and Simin Mahmoodifar for comments on the manuscript. L.K. is supported by NASA under award number NNG06EO90A. The authors thank the International Space Science Institute in Bern, Switzerland for hosting an International Team on X-ray bursts. This work benefited from events supported by the National Science Foundation under Grant No. PHY-1430152 (JINA Center for the Evolution of the Elements).

REFERENCES

- Arnett, W. D., Meakin, C., Viallet, M., Campbell, S. W., Lattanzio, J. C., & Mocák, M. 2015, *ApJ*, 809, 30
- Boirin, L., Keek, L., Méndez, M., Cumming, A., in 't Zand, J. J. M., Cottam, J., Paerels, F., & Lewin, W. H. G. 2007, *A&A*, 465, 559
- Brown, E. F., & Cumming, A. 2009, *ApJ*, 698, 1020
- Clayton, D. D. 1968, *Principles of stellar evolution and nucleosynthesis*, ed. Clayton, D. D.
- Cornelisse, R., et al. 2003, *A&A*, 405, 1033
- Cox, A. N. 1965, *Stellar Structure - Stars and Stellar Systems*, 195
- Cox, A. N., & Stewart, J. N. 1970a, *ApJS*, 19, 243
- . 1970b, *ApJS*, 19, 261
- Cox, J. P., & Whitney, C. 1958, *ApJ*, 127, 561
- Deibel, A., Cumming, A., Brown, E. F., & Page, D. 2015, *ApJ*, 809, L31
- Deibel, A., Meisel, Z., Schatz, H., Brown, E. F., & Cumming, A. 2016, *ApJ*, 831, 13
- Fisker, J. L., Schatz, H., & Thielemann, F.-K. 2008, *ApJS*, 174, 261
- Fujimoto, M. Y. 1988, *A&A*, 198, 163
- Fujimoto, M. Y., Sztajno, M., Lewin, W. H. G., & van Paradijs, J. 1987, *ApJ*, 319, 902
- Galloway, D. K., Muno, M. P., Hartman, J. M., Psaltis, D., & Chakrabarty, D. 2008, *ApJS*, 179, 360
- Gottwald, M., Haberl, F., Parmar, A. N., & White, N. E. 1987, *ApJ*, 323, 575
- Gupta, S., Brown, E. F., Schatz, H., Möller, P., & Kratz, K.-L. 2007, *ApJ*, 662, 1188
- Haensel, P., & Zdunik, J. L. 1990, *A&A*, 227, 431
- . 2003, *A&A*, 404, L33
- Heger, A., Woosley, S. E., & Spruit, H. C. 2005, *ApJ*, 626, 350

- Iben, Jr., I. 1975, *ApJ*, 196, 525
- Iglesias, C. A., & Rogers, F. J. 1996, *ApJ*, 464, 943
- Inogamov, N. A., & Sunyaev, R. A. 2010, *Astronomy Letters*, 36, 848
- Itoh, N., Uchida, S., Sakamoto, Y., Kohyama, Y., & Nozawa, S. 2008, *ApJ*, 677, 495
- José, J., Moreno, F., Parikh, A., & Iliadis, C. 2010, *ApJS*, 189, 204
- Keek, L., Cyburt, R. H., & Heger, A. 2014, *ApJ*, 787, 101
- Keek, L., Galloway, D. K., in 't Zand, J. J. M., & Heger, A. 2010, *ApJ*, 718, 292
- Keek, L., & Heger, A. 2011, *ApJ*, 743, 189
- Keek, L., Langer, N., & in 't Zand, J. J. M. 2009, *A&A*, 502, 871
- Kerstein, A. R. 1991, *Journal of Fluid Mechanics*, 231, 361
- Kippenhahn, R., & Weigert, A. 1994, *Stellar Structure and Evolution*
- Langer, N., Fricke, K. J., & Sugimoto, D. 1983, *A&A*, 126, 207
- Lewin, W. H. G., van Paradijs, J., & Taam, R. E. 1993, *Space Science Reviews*, 62, 223
- Lewin, W. H. G., et al. 1976, *MNRAS*, 177, 83P
- Linares, M., Altamirano, D., Chakrabarty, D., Cumming, A., & Keek, L. 2012, *ApJ*, 748, 82
- Malone, C. M., Nonaka, A., Almgren, A. S., Bell, J. B., & Zingale, M. 2011, *ApJ*, 728, 118
- Malone, C. M., Zingale, M., Nonaka, A., Almgren, A. S., & Bell, J. B. 2014, *ApJ*, 788, 115
- Motta, S., et al. 2011, *MNRAS*, 414, 1508
- Murakami, T., et al. 1980, *PASJ*, 32, 543
- Piro, A. L., & Bildsten, L. 2007, *ApJ*, 663, 1252
- Rauscher, T., Heger, A., Hoffman, R. D., & Woosley, S. E. 2002, *ApJ*, 576, 323
- Rauscher, T., & Thielemann, F.-K. 2000, *Atomic Data and Nuclear Data Tables*, 75, 1
- Schatz, H., et al. 2014, *Nature*, 505, 62
- Strohmayer, T., & Bildsten, L. 2006, *New views of thermonuclear bursts (Compact stellar X-ray sources)*, 113–156
- Turlione, A., Aguilera, D. N., & Pons, J. A. 2015, *A&A*, 577, A5
- Wallace, R. K., & Woosley, S. E. 1981, *ApJS*, 45, 389
- Weaver, T. A., Zimmerman, G. B., & Woosley, S. E. 1978, *ApJ*, 225, 1021
- Woosley, S. E., et al. 2004, *ApJS*, 151, 75
- Zhang, Q. S. 2013, *ApJS*, 205, 18
- Zingale, M., Malone, C. M., Nonaka, A., Almgren, A. S., & Bell, J. B. 2015, *ApJ*, 807, 60